Protein nanoparticles are nontoxic, tuneable cell stressors

ABSTRACT

Nanoparticle-cell interactions can promote cell toxicity and stimulate particular behavioural patterns, but cell responses to protein nanomaterials have been poorly studied. By repositioning oligomerization domains in a simple, modular self-assembling protein platform, we have generated closely related but distinguishable homomeric nanoparticles. Composed by building blocks with modular domains arranged in different order, they share amino acid composition. These materials, once exposed to cultured cells, are differentially internalized in absence of toxicity and trigger distinctive cell adaptive responses, monitored by the emission of tubular filopodia and enhanced drug sensitivity. The capability to rapidly modulate such cell responses by conventional protein engineering reveals protein nanoparticles as tuneable, versatile and potent cell stressors for cell-targeted conditioning.

Plain Language Summary

Protein nanoparticles have been unexpectedly found as able to induce adaptive responses in exposed cells, involving morphological and functional changes, in absence of toxicity. These responses can be tuned by conventional protein engineering of the building blocks and adapted and exploited in the context of molecular therapies.

Keywords

Recombinant proteins; nanoparticles; self-assembling; stressor; molecular therapy

INTRODUCTION

Proteins are gaining interest as safe and efficient biomaterials in different biomedical scenarios such as tissue engineering and drug delivery. In this context, nanoparticles, fibres, ribbons and 2D and 3D structures such as layers and hydrogel matrices are being recently developed. In contrast to metals, ceramics and polymers, whose biosafety and environmental impact might be controversial, proteins offer unique biocompatibility and full biodegradability, easy scalable bioproduction and high structural and functional versatility [1]. Being defined by the primary amino acid sequence, structure and function can be then modified by conventional genetic engineering. More than thirty years of experience in recombinant DNA technologies has offered more than 400 protein-based recombinant drugs approved for uses in humans by the medicines agencies [2] and hundreds of enzymes usable in different industries (food, textile, detergents, biofuel and paper, plus in chemical industry and for biomolecular research)[3]. In the last decades, many approaches have been explored to produce proteins as building blocks of complex supramolecular entities by engineering them as building blocks capable of self-assembling. This can be achieved by exploring natural oligomerization domains [4, 5] or by *de novo* designing molecular principles to promote very precise protein-protein interactions to build, for instance, cyclic structures, protein cages and others [6-9]. In this context, the combined use of a cationic domain at the amino terminus and a histidine-rich region at the carboxy terminus of a core protein (irrespective of the origin and amino acid sequences involved) has resulted in the generation of recombinant, protein-only cyclic nanoparticles ranging from 12 to 100 nm [10]. This category of materials has been demonstrated to be highly efficient as antimicrobial agents [11], as cell-targeted nanocarriers, drugs, and imaging agents in colorectal cancer [10, 12] and breast cancer [13] models and as blood-brain-barrier crossing vehicles [14].

Despite the architectonic robustness and wide applicability of such three-module architectonic platform [15], how nanoscale architecture and functionalities of nanoparticles could be modulated by the repositioning of these structural agents has been so far unexplored. We have redesigned here a paradigmatic building block based on an amino terminal polyarginine tail (R9), an enhanced GFP and a carboxy-terminal histidine-rich region (H6) into structural and functional isoforms. Showing slightly different bio-physical properties, these materials, that share their amino acid composition, promote different adaptive responses in exposed mammalian cells. The sensitivity and morphological plasticity of mammalian cells to nanoscale protein materials observed here is discussed envisaging how protein nanoparticles can be

designed to act as potent cell stressors or activators for pre-defined biomedical applications.

MATERIALS AND METHODS

Protein production

The three proteins used in this study were named according to the position of the peptides in the sequence (Figure 1A), and were all produced in *Escherichia coli* Rosetta (DE3). The parental protein R9-GFP-H6 has been previously described [16]. Two related protein constructions (H6-GFP-R9 and H6-R9-GFP) are modified versions that maintain the modular organization but with alternative order of peptides in the sequence. The encoding genes were designed in-house and were both supplied by Geneart (Germany) as *E. coli* codon-optimized genes. Upon insertion into pET22b (Novagen 69744-3), transformed bacteria were cultured in Lysogeny broth (LB) containing 34 g/ml chloramphenicol, 12.5 g/ml tetracycline (strain resistance) and 100 g/ml ampicillin (vector resistance), at 37 ºC and at 250 rpm shaking until an OD550 of ~0.6 units. Then, gene expression was induced with 1 mM isopropyl-b-D-thiogalactopyronaside (IPTG) and cells were cultured for 3 additional hours at 37 ºC and 250 rpm. After low speed centrifugation cells were resuspended in Wash buffer (20 mM Tris pH 8.0, 500 mM NaCl, 10 mM Imidazole) in the presence of EDTA-Free protease inhibitor cocktail (Complete EDTA-Free; Roche). R9-GFP-H6 expressing cells were further disrupted at 1200 Psi using a French Press (Thermo FA-078A). H6-GFP-R9 and H6-R9-GFP expressing cells were washed with 20 mM Tris pH 7.2, 1 M NaCl, 10 mM Imidazole in the presence of EDTA-Free protease inhibitor cocktail, and disrupted by sonication. The soluble fractions were in all cases collected and filtered through 0.22 µm-filter, to be purified by single-step His-based affinity chromatography in HiTrap Chelating HP 1 ml column (GE Healthcare) on an ÄKTA purifier (GE Healthcare). Elution was achieved by a linear gradient up to 500 mM Imidazole in the corresponding Wash buffer of each protein. R9-GFP-H6 was dialysed overnight at 4 ºC against Tris Dextrose buffer (20 mM Tris pH 7.4, 5 % dextrose), while H6-GFP-R9 and H6-R9-GFP were dialysed against 20 mM Tris pH 7.2, 500 mM NaCl, 5 % dextrose. The purity of the proteins was determined by denaturing SDS-polyacrylamide gel electrophoresis (12 % polyacrylamide) and anti-6x-His-tag Western Blot and Bradford's assays were performed to determine proteins' concentration using Bovine Serum Albumin as standard. Protein production has been partially performed by the ICTS "NANBIOSIS", more specifically by the Protein Production Platform of CIBER-BBN/IBB at the UAB sePBioEs scientific-technical service (http://www.nanbiosis.es/unit/u1-protein-production-platform-ppp/) .

Fluorescence determination and dynamic light scattering (DLS)

Specific fluorescence of proteins was determined in a Varian Cary Eclipse Fluorescence Spectrophotometer (Agilent Technologies) with all proteins being diluted to the same concentration (0.1 mg/ml). Samples were excited at a wavelength of 488 nm and the emission detected in the range 500-548 nm, with maximum emission detected at 510 nm. Volume size distribution of nanoparticles and monomeric proteins were determined by DLS at 633 nm (Zetasizer Nano ZS, Malvern Instruments Limited). Measurements were performed in triplicate.

Ultrastructural characterization

Morphometry (size and shape) of representative nanoparticles at nearly native state was evaluated with a Field emission scanning electron microscope (FESEM) Zeiss Merlin (Zeiss) operating at 1 kV. Drops of 3 µl of proteins were directly deposited on silicon wafers (Ted Pella Inc.) for 1 min, the excess was blotted with Whatman filter paper number 1 (GE Healthcare), air dried, and immediately observed without coating with a high resolution in-lens secondary electron detector. On the other hand, two sets of HeLa cultures were incubated alone or exposed to each protein construct in 24-well plates on a coverglass, and evaluated at 2 h and 24 h. One set of samples was processed for Scanning electron microscopy (SEM) ultrastructural visualization following standard procedures for mammalian cell cultures [17]. Briefly, coverglasses with each sample were fixed in 2.5 % (v/v) glutaraldehyde (Merck) and 2 % paraformaldehyde (TAAB) in 0.1 M phosphate buffer (PB; Sigma-Aldrich) for 2 h at 4 ºC, post-fixed in 1 % (w/v) osmium tetroxide (TAAB) containing 0.8 % (w/v) potassium hexocyanoferrate (Sigma-Aldrich) in PB for 2 h, and, then, dehydrated in graded series of ethanol, dried with CO_2 in a Bal-Tec CPD030 critical-point dryer (Balzers), mounted in stubs, coated with Pt-C, and observed in a SEM Zeiss EVO equipped with a secondary electron (SE) detector and operating at 15 kV. For the quantitative approach of morphological changes, SE images of randomly selected fields were captured and the percentage of cells with long filopodia (higher than the cell diameter) was calculated for each 24 h samples. The other set of samples was processed for FESEM immunolocalization visualization following standard procedures for gold labelling of mammalian cell cultures [18]. Briefly, coverglasses with each sample were fixed in 4 % paraformaldehyde (TAAB) in 0.1M PB (Sigma-Aldrich) for 30 min at 4 ºC, rinsed with 0.1 M PB and then placed in blocking buffer PBS- 1 % BSA (Sigma-Aldrich) containing 20 mM glycine (Merck), incubated overnight in a rabbit polyclonal anti-GFP primary antibody (ab-6556, dilution 1:25; Abcam) at 4 ºC, rinsed with PBS-BSA, incubated in protein A coupled to 20-nm gold particles (dilution 1:50; BBI) for 1 h at room temperature, rinsed with PBS and with water, and, then, dehydrated in graded series

of ethanol, dried with CO_2 in a Bal-Tec CPD030 critical-point dryer (Balzers), mounted in stubs, and observed without coating in a FESEM Zeiss Merlin operating at 1.4 kV and equipped with a secondary electron detector and an energy selective back-scattered electron (BSE) detector. For the quantitative approach of labelling, BSE images at same conditions (Mag: 60,000x, WD: 3 mm) of five different randomly selected fields of each 24 h sample were processed using Image J software (NIH Image).

Cell culture and internalization

In vitro experiments were performed on HeLa cells (ATCC-CCL-2) cultured in MEM-alpha (Gibco) supplemented with 10 % Foetal Calf Serum (Gibco) and incubated at 37ºC and 5 % CO_2. Internalization assays were performed in triplicate, in 24-well plates with the medium being replaced by serum-free OptiPro supplemented with L-Glutamine before the addition of the proteins. After incubation (2 h or 24 h, with varying concentrations of proteins as indicated in each case), a harsh treatment with trypsin was performed (Trypsin (Gibco), at 1 mg/ml for 15 min) to remove proteins bound to the surface of the cells. Internalization was analysed by flow cytometry on a FACS Canto (Becton Dickinson), with fluorescence excited using a 15 mW air-cooled argon ion laser at 488 nm and detected by a 530/30 nm band pass filter D detector. All internalization results were corrected with the fluorescence values obtained by fluorometry to render data comparable in terms of protein mass. To assess the level of involvement of CXCR4 receptors in internalization, competition assays were performed with HeLa cells pre-incubated for 1 h with the specific antagonist AMD3100 (octahydrochloride hydrate, Sigma-Aldrich), which was added to fresh OptiPRO medium to a final concentration of 10 µM (corresponding to 1:10 molar ratio protein:antagonist).

Cell viability assays

The potential toxicity of proteins was determined in HeLa cells cultured on 96-well Optical-Bottom plates with polymer base (Thermo Fisher Scientific) at 5,000 cells/well with 90 µl of MEM alpha medium with serum, for 24 h. Proteins prepared in 10 µl of medium for a final concentration of 1 µM or 2 µM were added to each well, and incubated for 2 h or 24 h. Then, cell viability was determined by CellTiter-GloLuminiscent Cell Viability Assay (Promega), by adding 100 µl of the reagent in each well. Luminescence was measured with Victor3 (PerkinElmer) according to the following program: 2 min of orbital shaking to induce cell lysis and 10 min of incubation

at RT to stabilize the luminescent signal, that was finally measured at 0.2 s, 0.5 s and 1 s.

The cell proliferation assay EZ4U (Biomedica) was used to determine the sensitivity of HeLa cells to cisplatin, after pre-conditioning with protein nanoparticles. Cells were cultured in a 96-well plate at 3,500 cells/well during 24 h at 37 ºC until reaching 70 % confluence. R9-GFP-H6 and H6-GFP-R9 nanoparticles were then added for 24 h at 37ºC to a final concentration of 2 µM. Then, the cytotoxic drug cisplatin (Sigma-Aldrich) was added at 40 µM and 65 µM for 24 h at 37 ºC. Finally, 20 µl of the assay substrate were added at 37ºC for 3 h and the absorbance was measured by a microplate-reader set at 450 nm with 620 nm as a background reference. All cell viability analyses were performed in triplicate.

Confocal microscopy

HeLa cells were grown on Mat-Tek plates (MatTek Corporation). The medium was replaced by serum-free OptiPro supplemented with L-Glutamine, followed by the addition of proteins to a final concentration of 1 µM or 2 µM, and further incubation for 2 h or 24 h before being washed in PBS buffer (Sigma-Aldrich). The nuclei were labelled with 10 µg/ml Hoechst 33342 (Invitrogen) and the plasma membrane with 2.5 µg/ml CellMask^{TM}Deep Red (Molecular Probes) for 10 min at RT and then washed in PBS buffer (Sigma-Aldrich). Living cells were recorded by TCS-SP5 confocal laser microscopy (Leica Microsystems) using a Plan Apo 63x/1.4 (oil HC x PL APO lambda blue) objective. Hoechst 33342 DNA label was excited with a blue diode (405 nm) and detected in the 415–460 nm range. GFP-proteins were excited with an Ar laser (488 nm) and detected in the 525–545 nm range. CellMask was excited with a HeNe laser (633 nm) and detected in the 650–775 nm range. To determine the protein localization inside the cell, stacks of 20–30 sections were collected with 0.5 µm of thickness, and 3D models were generated using Imaris software (Bitplane). Experiments were performed in quintuplicate, evaluating 4 fields of each experiment in 3D.

Statistical analysis

Values are expressed as mean data and standard error. Multiple comparisons were performed by one-way ANOVA with Tukey test or Kruskall-Wallis *H*-tests and pairwise comparisons by two-tailed Student *t*-tests or Mann-Whitney *U*-tests using Microsoft Excel 2011 or Past. Significant differences were accepted at $p<0.05$.

RESULTS

R9-GFP-H6, H6-GFP-R9 and H6-R9-GFP (Figure 1A) were successfully produced in *E. coli* as single protein species with the expected molecular mass of 30 kDa, a fact that was confirmed by conventional PAGE followed by ComassieBlue staining and Western Blot (Figure 1B). The observation of single bands was indicative of absence of important proteolysis. Upon successful purification by one step His-based affinity chromatography, all the proteins resulted fluorescent, proving a correct conformation of the GFP fluorophore and allowing the further monitoring of the materials in complex media. Noticeably, R9-GFP-H6 exhibited a slightly higher specific emission than its counterparts (Figure 1C). As previously demonstrated for R9-GFP-H6 [16], H6-GFP-R9 and H6-R9-GFP also self-assembled as nanostructures (Figure 1 D, Figure 2), with larger peak sizes and slightly wider size dispersion (59 nm and 79 nm, *versus* 28 nm in the case of R9-GFP-H6). As determined by FESEM, all the materials organized as regular nanoparticles with distinguishable and well defined toroid-like morphologies (Figure 2), confirming the sizes of the particles determined by DLS. In this regard, both DLS and FESEM have been recently observed as very robust analytical tools to precisely examine the nanoscale structure of protein-based assemblies, offering data fully coincident with more sophisticated methodologies such as SAXS, AFM, TEM (negative staining and Pt evaporation), and cryoTEM [10, 15, 16, 19]. H6-GFP-R9 and H6-R9-GFP were within the particle size ranges optimal for cell internalization [20] and also matching those reported to elicit cell responses [20]. R9-GFP-H6 was slightly below these effective reported sizes, although it has been previously shown that it efficiently internalizes cultured cells through the cell penetrating activities of R9 [21].

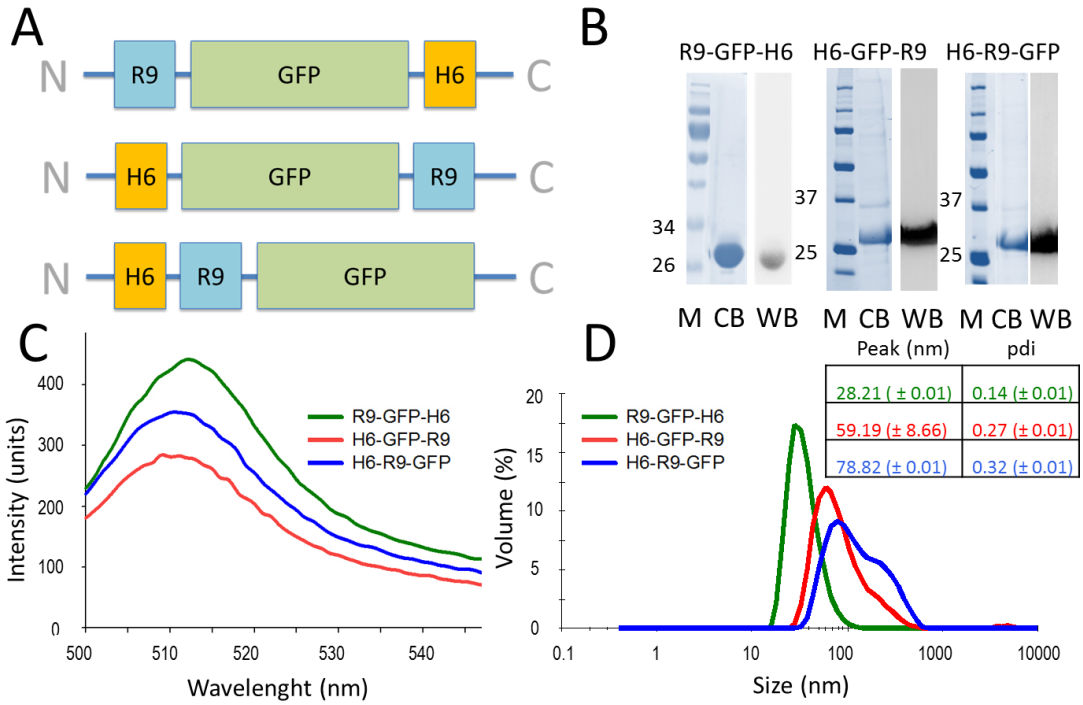

Figure 1. Biological production or protein building blocks and physical characterization of the resulting nanoparticles. A. Modular organization of R9-GFP-H6, H6-GFP-R9 and H6-R9-GFP (from top to bottom). A linker sequence (GGGNS) was always present at the amino terminus of GFP separating it from the previous module. B. Comassie Blue staining (CB) and Western blot (WB) of R9-GFP-H6, H6-GFP-R9 and H6-R9-GFP upon purification. Figures indicate the molecular masses of relevant markers (M) in kDa. C. Fluorescence emission spectra of purified R9-GFP-H6, H6-GFP-R9 and H6-R9-GFP, with all samples at the same concentration (0.1 mg/ml). D. Volume distribution analysis of R9-GFP-H6, H6-GFP-R9 and H6-R9-GFP nanoparticles.

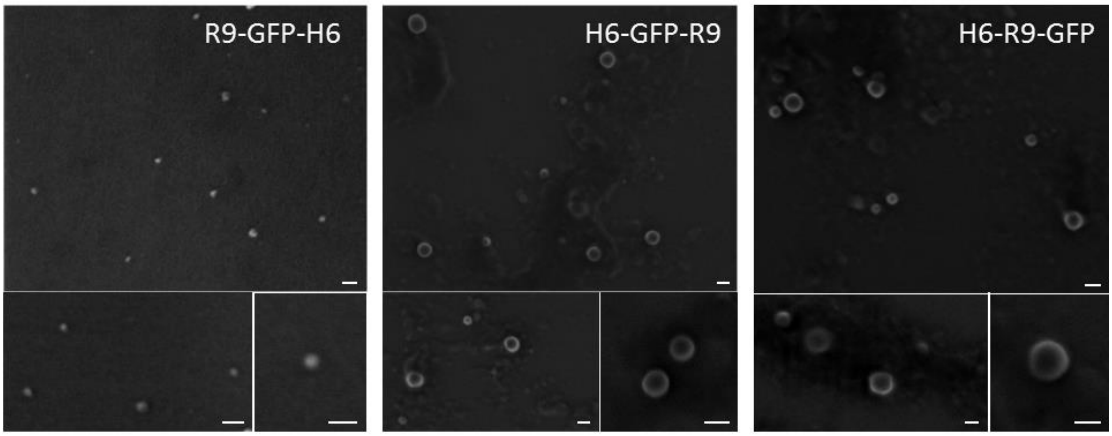

Figure 2. Morphometric analysis of protein nanoparticles. Representative FESEM imaging of ultrastructure (size and shape) of R9-GFP-H6, H6-GFP-R9 and H6-R9-GFP nanoparticles at different magnifications. Bars represent 60 nm.

Apart from its role as promoter of nanoparticle formation [16], R9 is a potent cell-penetrating peptide (CPP) that has been largely used in non-viral gene or protein therapies to mediate internalization of cargo drugs [22]. R9 might also have a residual receptor-specific penetrability through its interaction with the cytokine receptor CXCR4 [23], that is clinically relevant as a co-receptor of the human immunodeficiency virus [24] and also as a tumor marker overexpressed in several human cancers [25]. Internalization of the variant nanoparticles was then explored in cultured $CXCR4^+$ HeLa cells to investigate the effects that the R9 positioning in the modular constructs might have on R9-mediated cell penetrability. Interestingly, while all the material isoforms penetrated cells, the amount of internalized H6-GFP-R9 was 10 fold higher (and statistically significant) than that achieved by R9-GFP-H6 and H6-R9-GFP, as observed at both 2 h and 24 h of exposure to cells (Figure 3A). A dose-dependent penetration was evident and significant in all cases, but more consistently observed in poorly penetrating materials. To test the potential specificity mediating nanoparticle penetration, we used a chemical antagonist of CXCR4, namely AMD3100 [26], that blocks the interaction of the receptor with external ligands. This competitor significantly reduced the internalization of both R9-GFP-H6 and H6-R9-GFP at two tested doses, while it did not show negative effect on the uptake of H6-GFP-R9 (Figure 3B). This fact indicates an important extent of CXCR4-mediated cell penetrability of R9-GFP-H6 and H6-R9-GFP, while the uptake of H6-GFP-R9 relies mostly on mechanisms irrespective of CXCR4. Therefore, the free carboxy terminus of R9 as accommodated in H6-GFP-R9 mediates a dramatic enhancement of the uptake efficiency probably linked to the polyarginine acting as a true CPP, devoid of any specificity in the interaction with cells. In this context, it must be noted that at high concentrations of this protein and upon long exposure times, AMD3100, blocking CXCR4 binding, seems to favour a more efficient cell penetration by CXCR4-independent ways, probably through the CPP properties of R9 (Figure 3 B). Both events, cell penetrability and lack of specificity are apparently connected, since CXCR4-dependence is gained in nanoparticles with R9 in positions alternative to the carboxy terminus. Differential and enhanced cell penetration of H6-GFP-R9 was fully confirmed by confocal microscopy and by comparative analyses of internalized fluorescence (Figure 4A). In all treated cell cultures, a similar cell density, cell size and shape were observed. However, H6-GFP-R9 exposed cells, specially upon 24 h of exposure, showed abundant intracellular accumulation of fluorescence (Figure 4, B-D). Because of the high green intensity shown in such conventional confocal sections of the highly penetrating nanoparticle we performed further analysis and 3D reconstructions to better explore the occurrence and status of the intracellular protein. As observed (Figure 4B, D), the H6-GFP-R9

partially appeared as rod-shaped or tubular structures that might be due to longitudinal staking of toroid nanoparticles (as previously observed for R9-GFP-H6 under specific conditions such as the presence of DNA [27]), or to a particular organization of cellular membranes to which fluorescent material is associated. Shorter exposures (2 hours) were valuated (Figure 4D), where proteins highly colocalize with cell membrane, and elongated filopodia can be observed associated with proteins. The 3D reconstruction (Figure 4E) shows protein distribution. In figures 4E and 4F we can observe that under the same conditions the proteins R9-GFP-H6 and H6-R9-GFP, respectively, have an inferior penetration capacity, occurring as dots but never as elongated structures. The penetrability of the materials was not, in any case, linked to cytotoxicity, as exposed cells did not show any significant decrease in cell viability (Figure 4H). No important aggregation could be associated to H6-GFP-R9 as no large fluorescent clusters were apparent in the extracellular media. Although from these images it was not possible to precisely discriminate between intra and extracellular localization of these fibrils, most of the recorded fluorescence was indeed intracellular (Figure 4A).

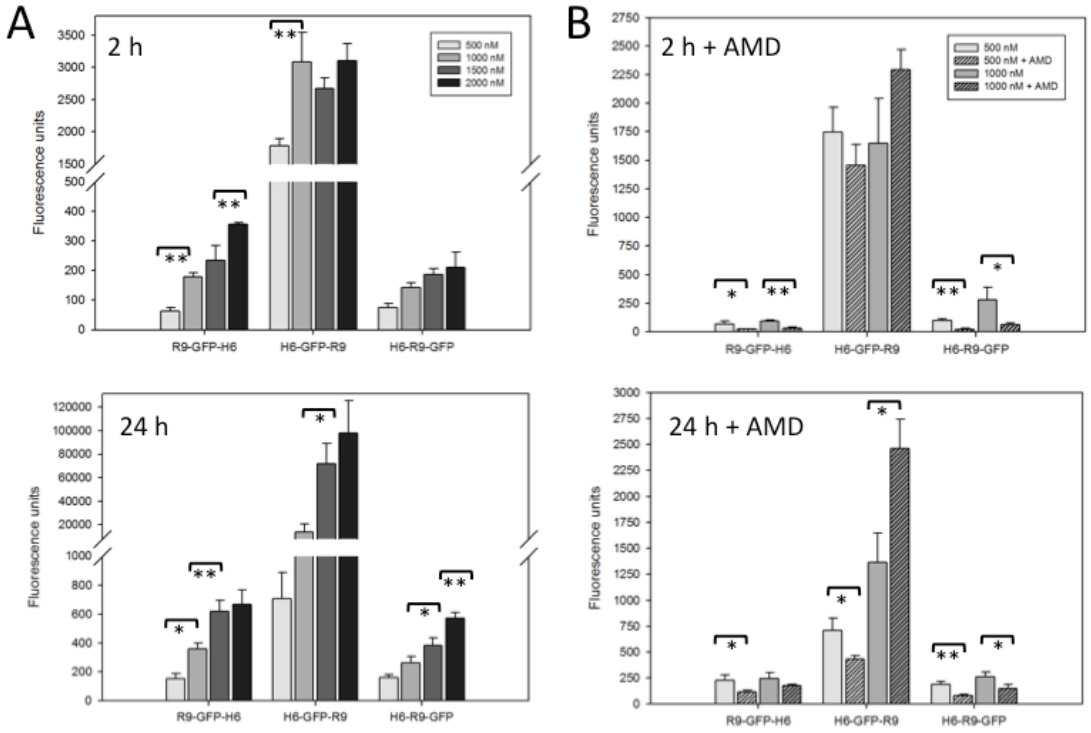

Figure 3. Cell penetrability of protein nanoparticles. A. Intracellular fluorescence after 2 hours and 24 hours of exposure of cultured HeLa cells to different amounts of protein nanoparticles. Intracellular fluorescence was recorded after a harsh trypsin treatment to fully remove externally retained signal [28], and the records were corrected by the specific fluorescence of the protein variants (Figure 1C) to allow mass-based comparisons. Statistics are ** $p<0.001$; * $p<0.05$. Pairwise comparisons between R9-GFP-H6 and H6-GFP-R9, and between H6-GFP-R9 and H6-R9-GFP always resulted significant for any tested dose (always **,

at exception of 1000 mM and 24 h, that resulted in *). Comparisons between R9-GFP-H6 and H6-R9-GFP resulted always not significant for any tested dose. B. AMD3100 (AMD)-mediated inhibition of nanoparticle internalization at 2 hours and 24 hours of exposure.

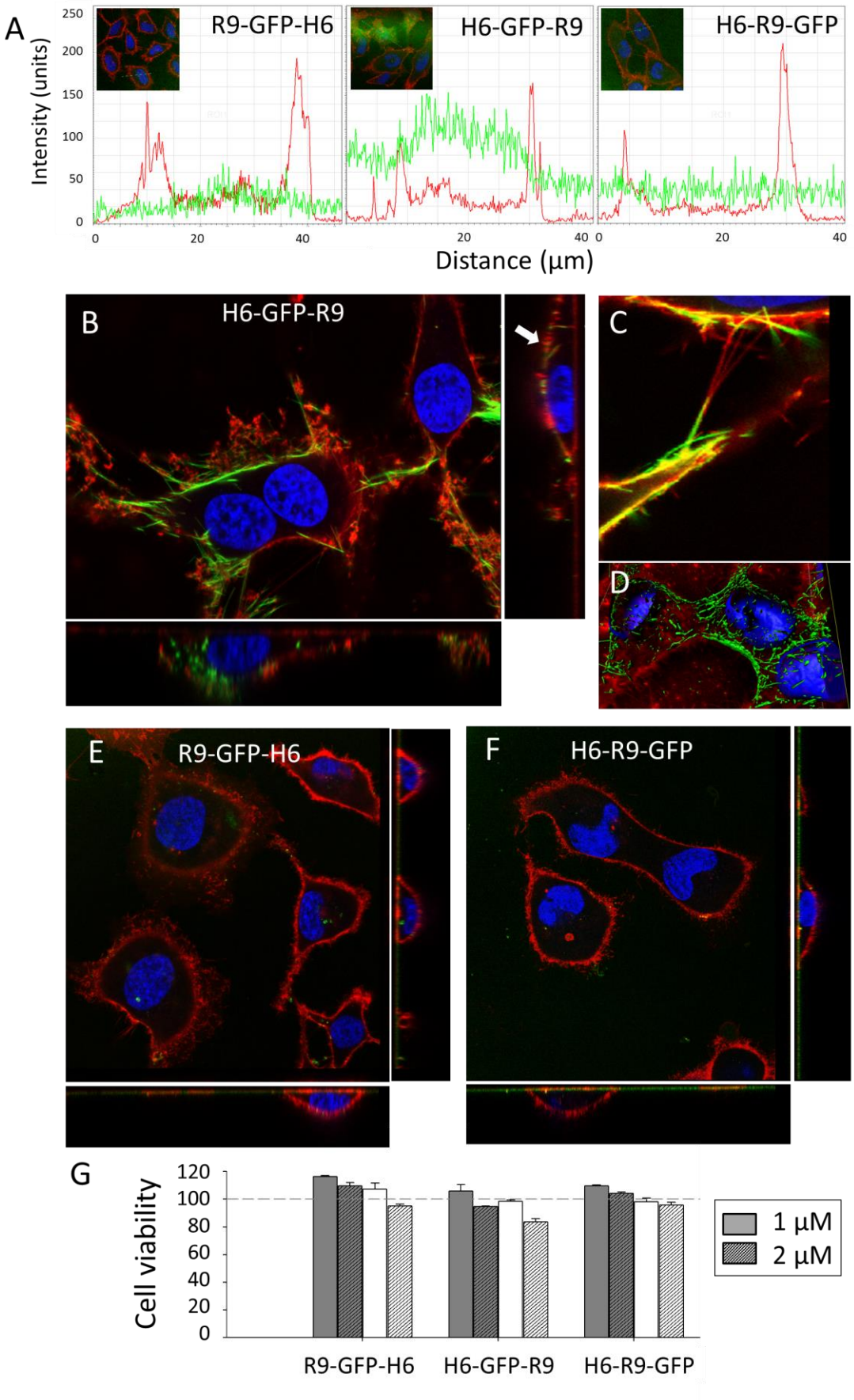
A
R9-GFP-H6
H6-GFP-R9
H6-R9-GFP
Intensity (units)
Distance (µm)
B
H6-GFP-R9
C
D
E
R9-GFP-H6
F
H6-R9-GFP
G
Cell viability
1 µM
2 µM
R9-GFP-H6
H6-GFP-R9
H6-R9-GFP

Figure 4. Internalization and intracelular localization of protein nanoparticles. A. Intracellular comparative profiling of green fluorescence (green lines) associated to nanoparticles in longitudinal confocal sections of exposed HeLa cells. The red line indicates the cell membrane intensity. In the insets, representative confocal images of the cultures 2h upon protein addition. B. Orthogonal views of the image volume of cells exposed to H6-GFP-R9 for 24 h, showing longitudinal fluorescent strips, some of which appeared inside the cell (white arrow). The blue and red signals correspond to nuclear and cell membrane labeling, respectively. C. Colocalization (yellowish merging of green and red signals) between the tubular proteins H6-GFP-R9 with the membrane filopodia. D. Imaris 3D reconstruction of the half volume of the cells shows the protein H6-GFP-R9 inside the cytoplasm. E-F. Orthogonal views of image volumes from R9-GFP-H6 and H6-R9-GFP, respectively. Protein constructs appeared as globular structures and show inferior penetration capacity inside the cell. G. MTT-mediated analysis of HeLa cell viability upon exposure to 1 and 2 µm nanoparticles for 2h in solid bars and 24 h in dashed bars. A Mann-Whitney test revealed non-significant differences between untreated and treated cell cultures (p=0.05).

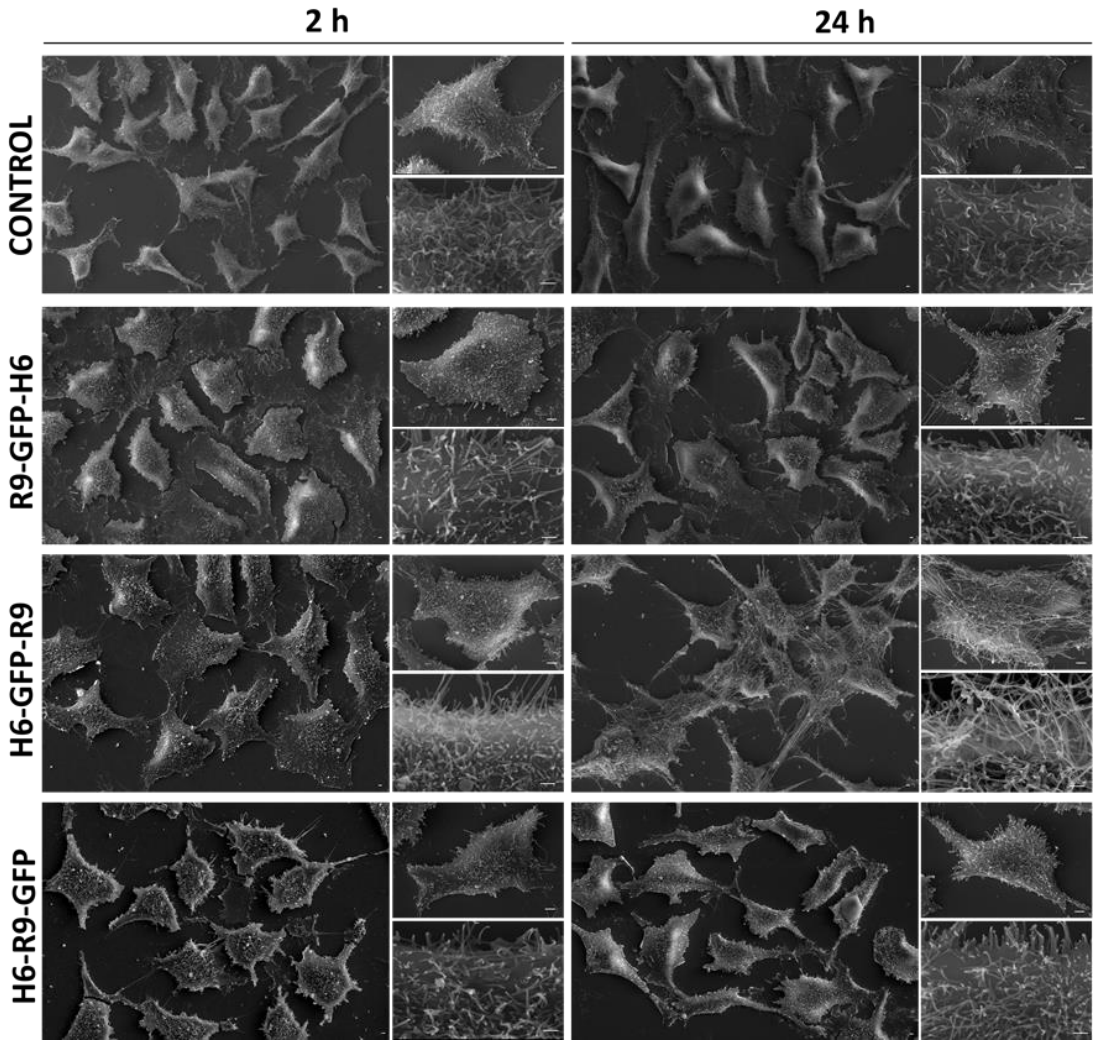

Figure 5. SEM analysis of cells exposed to nanoparticles. Representative SEM images of mammalian HeLa cells ultrastructure once incubated alone (control) or exposed to the three different constructs for two times (2 h and 24 h). Bars represent 1 µm.

Because of the observed particular fluorescence pattern, (Figure 4B), we decided to explore the ultrastructural morphology of nanoparticle-exposed cells by combining FESEM (SE), labelling of GFP (by quantification of gold particles from a secondary antibody -BSE-), and the localization of GFP labelling combined with morphometric data (SE+BSE). As observed (Figure 5), there was a dramatic increase in number and length of tubular membranous structures or filopodia (with diameters within the nanoscale) in HeLa cells upon contact with H6-GFP-R9 nanoparticles, especially after 24 h exposure (39.2 % of cells with filopodia lengths comparable to the cell diameter; n=56), but not in cultures exposed to alternative modular constructions (0 % in both cases; n=50). The absence of significant cell toxicity in any treatment (Figures 4H and 5) excluded the occurrence of cell-death pathways while prompted to speculate about the stimulation of cell sensing activities promoted by H6-GFP-R9. Interestingly, the analysis of protein immunolocalization by FESEM in exposed HeLa cells indicated the presence of external nanoparticles closely associated to tubular membrane structures, which is more apparent in the case of H6-GFP-R9.The heavy coating of filopodia with H6-GFP-R9 might be linked to the fibrilar fluorescent structures shown in Figure 4B. However, the high intracellular fluorescence emission of H6-GFP-R9-exposed cells (Figure 3, 4A) seemed to indicate that an important part of such fluorescent biomaterial had penetrated into cells.

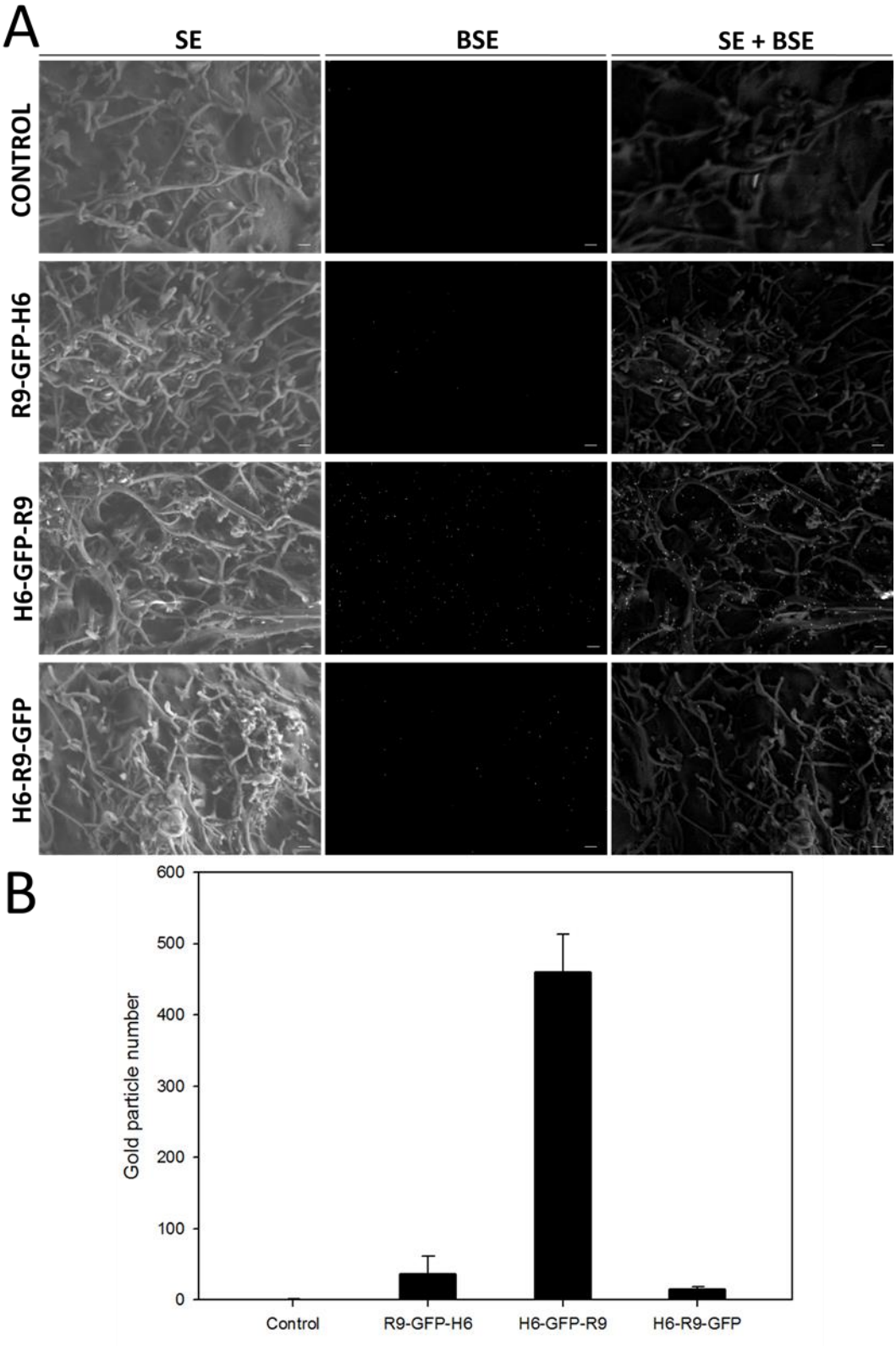

Figure 6: FESEM analysis of nanoparticles localization in cell surface. A. Representative FESEM images of nanoparticles localization at nanoscale in mammalian HeLa cells surface after incubation alone (control) or exposed 24 h to the three different constructs. Bars represent 200 nm. SE: secondary electron detection; BSE: energy selective back-scattered electron detection. B. Quantitative analysis of gold nanoparticles immune-associated to cell filopodia.

The formation of membranous tubes of 50-200 nm of diameter and up to several cell diameters long had been already described [29]. They might be derived from conventional filopodia and often contain F-actin [30]. Importantly, these membranous structures seem to be involved in molecular, electrical and mechanical signalling as well as in developmental processes [30]. In addition, they participate in the intercellular transfer of cellular components and are used by viruses and prions to spread between cells [30]. To investigate if transfer of substances might be affected in filopodia-emitting cells once stimulated by H6-GFP-R9 nanoparticles we evaluated the cytotoxic effect of cisplatin, to which normal cells are partially permeable. As observed, nanoparticle exposure moderately but significantly enhanced cell death mediated by this drug, at two different tested doses (Figure 7). This fact indicates that the cell-stressing effect of H6-GFP-R9 nanoparticles has a physiological counterpart beyond the mere morphological modification of exposed cells.

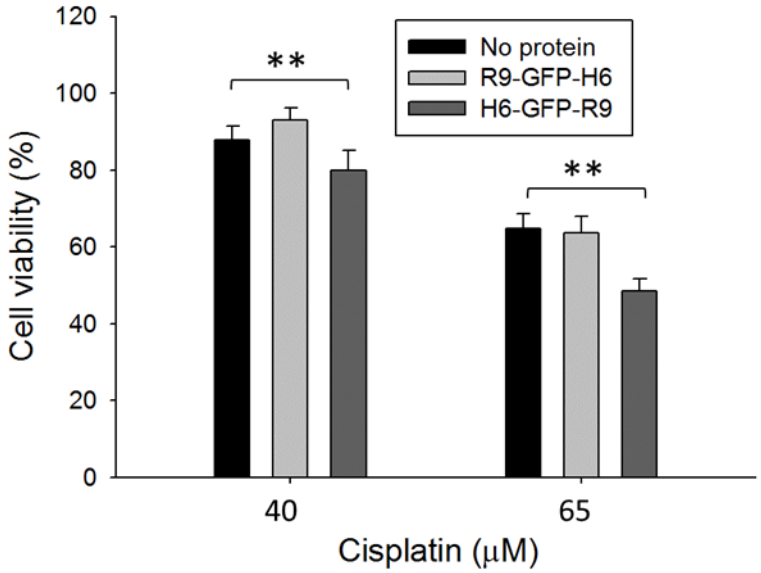

Figure 7. Cell sensitivity to different doses of cisplatin upon pre-conditioning R9-GFP-H6 or H6-GFP-R9 nanoparticles. Significant differences (**, p<0.001) are shown.

DISCUSSION

Physicochemical properties of nanoparticles such as size, shape, superficial charge and chemical composition determine the intricacy of material-cell interactions and the biological effects on exposed cells, including toxicity [31-34]. Less studied than toxicity, a spectrum of adaptive cell responses and compensatory systemic responses is triggered upon exposure to nanostructured materials [35], that might follow non-lineal, hormetic dose-response patterns [35, 36]. Systemic stress in response to nanoparticle exposure has been also reported, including increase of plasmatic cortisol levels [37] and stress hormones [38], autophagy [39], oxidative stress [40] and enhanced expression of apoptosis-related genes [41]. Nanostructured materials can be then observed as a category of cellular and organic stressors, whose biological effects are ultimately linked to their intrinsic toxicity [39, 42-44]. Most of these toxicity studies have been performed with metal nanoparticles, but toxicity and potential stress responses triggered by protein nanoparticles remain unexplored, despite of the emerging interest in this category of materials.

Regular protein-only nanoparticles are under fast development pushed by emerging rational and semi-rational principles to control self-assembly[5, 7, 9, 45], and among other applications they are appealing as virus-like mimetics for intracellular drug delivery [46]. In addition, protein-based nanomaterials benefit from easy biological fabrication and from the capability to recruit a diversity of functions relevant to drug delivery such as self-assembling, cell targeting, endosomal escape and nuclear transport in their building blocks [47]. Here we have produced and characterized, regarding architecture and function, closely related homomeric nanoparticles designed by repositioning oligomerization domains (R9 and H6) in self-assembling, modular polypeptides (Figure 1). By this, morphometrically distinguishable nanoparticles have been generated (Figure 2) that differentially penetrate cultured cells (Figure 3). In a particular domain distribution, in which R9 is placed at the carboxy terminus of the building block (H6-GFP-R9), nanoparticles show a dramatically enhanced cell penetrability associated to the CPP properties of R9 (Figure 3). In alternative modular distributions (R9-GFP-H6 and H6-R9-GFP), nanoparticles penetrate target cells by a combination of CXCR4-independent (CPP-based) and CXCR4-dependent internalization mechanisms (Figure 3). Therefore, the precise position of R9 may either favour or impair the display accessibility of this peptide to interact with the receptor CXCR4, which is particularly precluded when R9 is at the carboxy terminus.

Interestingly, the exposure to cultured cells to these materials, that share amino acid composition but show distinct nanoparticle size (indicative of different oligomeric complexity [15]), trigger differential emission of long tubular filopodia (Figure 5), that is especially intense in the case of the highly penetrating H6-GFP-R9 nanoparticles (Figure 3). Filopodia are actin-rich membrane emissions occurring in adaptive cell responses, which linked to stress fibres [48] serve cells to probe extracellular media. They also have pivotal roles in migration [49], neuronal differentiation and in tissue regeneration [50]. The particular formation of the membranous structures observed here (long tubules with nanoscale diameters) is mediated by the Ral-exocyst pathway [51] and is involved in intercellular transfer of materials, including viruses and prions [30].The localization of H6-GFP-R9 nanoparticles on these membranous emissions (Figure 6) reinforces the idea that the emission of filopodia occurs as a response to nanoparticle exposure and that protein nanoparticles act as cell stressors. This effect occurs by mechanisms that unlike metal nanoparticles, are fully unlinked to cell toxicity (Figure 4G) and might be related to the interaction between nanoparticles and plasma membrane that regulate CPP-mediated engulfment (Figure 3). The precise mechanisms by which H6-GFP-R9 nanoparticles stimulate filopodia emission are not known, although it is unlikely that they would be solely based on the material size. The size variation of the nanoparticle set studied here is within relatively narrow margins in which such response has not been previously described for biologically inert materials [20]. This fact suggests a position-dependent involvement of biologically active protein domains, such as R9. Interestingly cells emitting more and longer filopodia are those more sensitive when exposed to cisplatin (Figure 7). This might indicate a physiological connection between membrane morphology (determining the cell surface area) and drug penetrability, although a higher drug sensitivity of H6-GFP-R9-exposed cells, due to inner stress mechanisms cannot be fully discarded. Among other potential applications, this effect might be considered to amplify drug effects through previous cell pre-conditioning, which might be in addition targeted to cell surface tumor markers by empowering the nanoparticles with specific ligands of these markers. Since protein corona is not formed over protein nanoparticles, the *in vivo* tumor targeting of these materials once empowered by short peptide ligands is extremely precise [19].

Different extent of filopodia formation is achieved by members of the nanoparticle set, which differ from each other by mere modular organization of the building blocks. Therefore, irrespective of the precise underlying mechanisms, simple protein engineering can convert irrelevant nanoparticles such as R9-GFP-H6 into potent inducers of cell responses like H6-GFP-R9. This is probably related to an enhanced

membrane activity of R9 when showing a free carboxy terminus, maybe combined with an optimal material size. According to our data, nanoparticle-conditioned cells might be more permeable and/or more sensitive to external substances that, like cisplatin, might have a therapeutic applicability. The development of non-toxic cell stressors based on self-assembling proteins (that can be easily produced in food-grade bacterian absence of endotoxin contaminants [52]) can be further improved by cell targeting,reachable by the incorporation of specific cell surface ligands. These nanostructured biomaterials can then activate adaptive responses in target cells. This possibility points out protein nanoparticles (fully tuneable by genetic engineering) into appealing instruments in regenerative medicine, in cell-targeted therapies, and more generically, for the re-programming of adaptive cellular activities in therapeutic contexts.

SUMMARY POINTS

The relative position of R9 and H6 domains in GFP fusions impacts on the specific fluorescence emission of the modular polypeptides and on their ability to self-assemble as oligomeric nanoparticles.

The modular organization R9-GFP-H6 results in highly fluorescent 27 nm-nanoparticles, while H6-GFP-R9 and H6-R9-GFP assemble in less fluorescent, larger materials.

Penetrability of the oligomers in cultured cells, mediated by R9, is dramatically enhanced in the disposition H6-GFP-R9, regarding the alternative modular organizations. Cell penetrability of H6-GFP-R9 nanoparticles occurs irrespective of the cell receptor CXCR4 (at least at early exposure times), to which R9 has been proved to bind.

H6-R9-GFP but not the other tested protein variants stimulates, in exposed HeLa cells, an abundant emission of long and tubular filopodia in absence of detectable cytotoxicity.

In H6-GFP-R9-exposed cells, cisplatin is more cytotoxic than in cells exposed to other protein variants, by mechanisms that might involve enhanced drug penetrability and/or enhanced drug sensitivity.

Promoting protein oligomerization of protein nanoparticles by cationic and histidine-rich domain engineering allows the production of closely related protein materials but showing fully distinguishable biological activities.

By alternating the domain position in protein nanoparticles with the same amino acid composition it is possible to control adaptive cells responses. These protein materials

might be of interest as pre-conditioning agents in molecular therapy, regenerative medicine and other biomedical contexts.

References

1. Corchero JL, Vazquez E, Garcia-Fruitos E, Ferrer-Miralles N, Villaverde A. Recombinant protein materials for bioengineering and nanomedicine. *Nanomedicine* 9(18), 2817-2828 (2014).

2. Sanchez-Garcia L, Martin L, Mangues R, Ferrer-Miralles N, Vazquez E, Villaverde A. Recombinant pharmaceuticals from microbial cells: a 2015 update. *Microbial cell factories* 15 33 (2016).

3. Jemli S, Ayadi-Zouari D, Hlima HB, Bejar S. Biocatalysts: application and engineering for industrial purposes. *Critical reviews in biotechnology* 36(2), 246-258 (2016).

4. Yeates TO, Padilla JE. Designing supramolecular protein assemblies. *Current opinion in structural biology* 12(4), 464-470 (2002).

5. Ferrer-Miralles N, Rodriguez-Carmona E, Corchero JL, Garcia-Fruitos E, Vazquez E, Villaverde A. Engineering protein self-assembling in protein-based nanomedicines for drug delivery and gene therapy. *Critical reviews in biotechnology* 35(2), 209-221 (2015).

6. Yeates TO. Geometric Principles for Designing Highly Symmetric Self-Assembling Protein Nanomaterials. *Annual review of biophysics* doi:10.1146/annurev-biophys-070816-033928 (2017).

7. Yeates TO, Liu Y, Laniado J. The design of symmetric protein nanomaterials comes of age in theory and practice. *Current opinion in structural biology* 39 134-143 (2016).

8. Boyken SE, Chen Z, Groves B *et al*. De novo design of protein homo-oligomers with modular hydrogen-bond network-mediated specificity. *Science* 352(6286), 680-687 (2016).

9. Fallas JA, Ueda G, Sheffler W *et al*. Computational design of self-assembling cyclic protein homo-oligomers. *Nature chemistry* 9(4), 353-360 (2017).

10. Rueda F, Cespedes MV, Conchillo-Sole O *et al*. Bottom-Up Instructive Quality Control in the Biofabrication of Smart Protein Materials. *Advanced materials* 27(47), 7816-7822 (2015).

11. Serna N, Sanchez-Garcia L, Sanchez-Chardi A *et al*. Protein-only, antimicrobial peptide-containing recombinant nanoparticles with inherent built-in antibacterial activity. *Acta biomaterialia* doi:10.1016/j.actbio.2017.07.027 (2017).

12. Naroa Serna MVC, Laura Sánchez-García, Ugutz Unzueta, Rita Sala, Alejandro Sánchez-Chardi, Francisco Cortés, Neus Ferrer-Miralles, Ramón Mangues, Esther Vázquez and Antonio Villaverde. Peptide-Based Nanostructured Materials with Intrinsic Proapoptotic Activities in CXCR4+ Solid Tumors. *Advanced Functional Materials* doi:DOI: 10.1002/adfm.201700919 (2017).

13. Pesarrodona M, Ferrer-Miralles N, Unzueta U *et al*. Intracellular targeting of CD44+ cells with self-assembling, protein only nanoparticles*. International journal of pharmaceutics* 473(1-2), 286-295 (2014).

14. Serna N, Cespedes MV, Saccardo P *et al*. Rational engineering of single-chain polypeptides into protein-only, BBB-targeted nanoparticles*. Nanomedicine : nanotechnology, biology, and medicine* 12(5), 1241-1251 (2016).

15. Pesarrodona M, Crosas E, Cubarsi R *et al*. Intrinsic functional and architectonic heterogeneity of tumor-targeted protein nanoparticles*. Nanoscale* 9(19), 6427-6435 (2017).

16. Vazquez E, Roldan M, Diez-Gil C *et al*. Protein nanodisk assembling and intracellular trafficking powered by an arginine-rich (R9) peptide*. Nanomedicine* 5(2), 259-268 (2010).

17. Rueda F, Gasser B, Sanchez-Chardi A *et al*. Functional inclusion bodies produced in the yeast Pichia pastoris*. Microbial cell factories* 15(1), 166 (2016).

18. Seras-Franzoso J, Sanchez-Chardi A, Garcia-Fruitos E, Vazquez E, Villaverde A. Cellular uptake and intracellular fate of protein releasing bacterial amyloids in mammalian cells*. Soft matter* 12(14), 3451-3460 (2016).

19. Cespedes MV, Unzueta U, Tatkiewicz W *et al*. In vivo architectonic stability of fully de novo designed protein-only nanoparticles*. ACS nano* 8(5), 4166-4176 (2014).

20. Shang L, Nienhaus K, Nienhaus GU. Engineered nanoparticles interacting with cells: size matters*. J Nanobiotechnology* 12 5 (2014).

21. Vazquez E, Cubarsi R, Unzueta U *et al*. Internalization and kinetics of nuclear migration of protein-only, arginine-rich nanoparticles*. Biomaterials* 31(35), 9333-9339 (2010).

22. Saccardo P, Villaverde A, Gonzalez-Montalban N. Peptide-mediated DNA condensation for non-viral gene therapy*. Biotechnology advances* 27(4), 432-438 (2009).

23. Tanaka G, Nakase I, Fukuda Y *et al*. CXCR4 stimulates macropinocytosis: implications for cellular uptake of arginine-rich cell-penetrating peptides and HIV*. Chemistry & biology* 19(11), 1437-1446 (2012).

24. Chan DC, Kim PS. HIV entry and its inhibition*. Cell* 93(5), 681-684 (1998).

25. Burger JA, Kipps TJ. CXCR4: a key receptor in the crosstalk between tumor cells and their microenvironment*. Blood* 107(5), 1761-1767 (2006).

26. Kim HY, Hwang JY, Kim SW *et al*. The CXCR4 Antagonist AMD3100 Has Dual Effects on Survival and Proliferation of Myeloma Cells In Vitro*. Cancer research and treatment : official journal of Korean Cancer Association* 42(4), 225-234 (2010).

27. Unzueta U, Saccardo P, Domingo-Espin J *et al*. Sheltering DNA in self-organizing, protein-only nano-shells as artificial viruses for gene delivery*. Nanomedicine : nanotechnology, biology, and medicine* 10(3), 535-541 (2014).

28. Richard JP, Melikov K, Vives E *et al*. Cell-penetrating peptides. A reevaluation of the mechanism of cellular uptake*. The Journal of biological chemistry* 278(1), 585-590 (2003).

29. Derenyi I, Julicher F, Prost J. Formation and interaction of membrane tubes*. Physical review letters* 88(23), 238101 (2002).

30. Gerdes HH, Rustom A, Wang X. Tunneling nanotubes, an emerging intercellular communication route in development*. Mechanisms of development* 130(6-8), 381-387 (2013).

31. Albanese A, Tang PS, Chan WC. The effect of nanoparticle size, shape, and surface chemistry on biological systems*. Annual review of biomedical engineering* 14 1-16 (2012).

32. Cho EC, Au L, Zhang Q, Xia Y. The effects of size, shape, and surface functional group of gold nanostructures on their adsorption and internalization by cells*. Small* 6(4), 517-522 (2010).

33. Elsaesser A, Howard CV. Toxicology of nanoparticles*. Advanced drug delivery reviews* 64(2), 129-137 (2012).

34. Verma A, Stellacci F. Effect of surface properties on nanoparticle-cell interactions*. Small* 6(1), 12-21 (2010).

35. Bell IR, Ives JA, Jonas WB. Nonlinear effects of nanoparticles: biological variability from hormetic doses, small particle sizes, and dynamic adaptive interactions*. Dose-response : a publication of International Hormesis Society* 12(2), 202-232 (2014).

36. Sthijns MM, Thongkam W, Albrecht C *et al*. Silver nanoparticles induce hormesis in A549 human epithelial cells*. Toxicology in vitro : an international journal published in association with BIBRA* 40 223-233 (2017).

37. Teles M, Soares AM, Tort L, Guimaraes L, Oliveira M. Linking cortisol response with gene expression in fish exposed to gold nanoparticles*. Sci Total Environ* 584-585 1004-1011 (2017).

38. Vankova R, Landa P, Podlipna R *et al*. ZnO nanoparticle effects on hormonal pools in Arabidopsis thaliana*. Sci Total Environ* 593-594 535-542 (2017).

39. Peynshaert K, Manshian BB, Joris F *et al*. Exploiting intrinsic nanoparticle toxicity: the pros and cons of nanoparticle-induced autophagy in biomedical research*. Chemical reviews* 114(15), 7581-7609 (2014).

40. Ahmad J, Siddiqui MA, Akhtar MJ *et al*. Copper doping enhanced the oxidative stress-mediated cytotoxicity of TiO2 nanoparticles in A549 cells*. Human & experimental toxicology* doi:10.1177/0960327117714040 960327117714040 (2017).

41. Teles M, Fierro-Castro C, Na-Phatthalung P *et al*. Assessment of gold nanoparticle effects in a marine teleost (Sparus aurata) using molecular and biochemical biomarkers*. Aquatic toxicology* 177 125-135 (2016).

42. Kuku G, Culha M. Investigating the Origins of Toxic Response in TiO(2) Nanoparticle-Treated Cells. *Nanomaterials* 7(4), (2017).

43. Sarkar A, Ghosh M, Sil PC. Nanotoxicity: oxidative stress mediated toxicity of metal and metal oxide nanoparticles. *Journal of nanoscience and nanotechnology* 14(1), 730-743 (2014).

44. Manke A, Wang L, Rojanasakul Y. Mechanisms of nanoparticle-induced oxidative stress and toxicity. *BioMed research international* 2013 942916 (2013).

45. Doll TaPF, Dey R, Burkhard P. Design and optimization of peptide nanoparticles. *J Nanobiotechnol* 13 (2015).

46. Unzueta U, Cespedes MV, Vazquez E, Ferrer-Miralles N, Mangues R, Villaverde A. Towards protein-based viral mimetics for cancer therapies. *Trends in biotechnology* 33(5), 253-258 (2015).

47. Vazquez E, Mangues R, Villaverde A. Functional recruitment for drug delivery through protein-based nanotechnologies. *Nanomedicine* 11(11), 1333-1336 (2016).

48. Hotulainen P, Lappalainen P. Stress fibers are generated by two distinct actin assembly mechanisms in motile cells. *The Journal of cell biology* 173(3), 383-394 (2006).

49. Partridge MA, Marcantonio EE. Initiation of attachment and generation of mature focal adhesions by integrin-containing filopodia in cell spreading. *Molecular biology of the cell* 17(10), 4237-4248 (2006).

50. Mattila PK, Lappalainen P. Filopodia: molecular architecture and cellular functions. *Nature reviews. Molecular cell biology* 9(6), 446-454 (2008).

51. Hase K, Kimura S, Takatsu H *et al*. M-Sec promotes membrane nanotube formation by interacting with Ral and the exocyst complex. *Nature cell biology* 11(12), 1427-1432 (2009).

52. Cano-Garrido O, Cespedes MV, Unzueta U *et al*. CXCR4(+)-targeted protein nanoparticles produced in the food-grade bacterium Lactococcus lactis. *Nanomedicine* 11(18), 2387-2398 (2016).

* Shang L, Nienhaus K, Nienhaus GU. Engineered nanoparticles interacting with cells: size matters. J Nanobiotechnology 12 5 (2014).

Cytotoxicity and size-related effects of nanoparticles over exposed cells are deeply elaborated and discussed.

**Tanaka G, Nakase I, Fukuda Y et al. CXCR4 stimulates macropinocytosis: implications for cellular uptake of arginine-rich cell-penetrating peptides and HIV. Chemistry & biology 19(11), 1437-1446 (2012).

Polyarginies, apart from their ability to penetrate exposed cells by a unspecific CPP mechanism they can also enter via CXCR4, a cell surface cell marker relevant in metastatic cancer and in HIV infection

** Bell IR, Ives JA, Jonas WB. Nonlinear effects of nanoparticles: biological variability from hormetic doses, small particle sizes, and dynamic adaptive interactions. Dose-response: a publication of International Hormesis Society 12(2), 202-232 (2014).
Nanoparticles stimulate adaptive cell responses at low doses by nonlinear mechanisms.

* Naroa Serna MVC, Laura Sánchez-García, UgutzUnzueta, Rita Sala, Alejandro Sánchez-Chardi, Francisco Cortés, Neus Ferrer-Miralles, Ramón Mangues, Esther Vázquez and Antonio Villaverde. Peptide-Based Nanostructured Materials with Intrinsic Proapoptotic Activities in CXCR4+ Solid Tumors. Advanced Functional Materials 27, 1700919.
Self-assembling, cell-targeted protein nanoparticles can promote specific apoptosis in tumoral tissues, upon systemic administration, by intrinsic cytotoxic activities.